Sādhanā (2020) 45:189
https://doi.org/10.1007/s12046-020-01426-x

Self-heating of rolled ZnCuTi sheets

M MILESI[1,*], D PINO MUÑOZ[2], A LAGROUM[2], C PRADILLE[3] and P O BOUCHARD[2]

[1]VM Building Solutions, Les mercuriales, 40 rue Jean-Jaurès, 93176 Bagnolet Cedex, France
[2]MINES ParisTech, PSL Research University, CEMEF - Centre de mise en forme des matériaux, CNRS UMR 7635, CS 10207 rue Claude Daunesse, 06904 Sophia Antipolis Cedex, France
[3]Mat Xper, 19 traverse du Barri, 06560 Valbonne, France
e-mail: marc.milesi@vmzinc.com

MS received 1 October 2019; revised 12 May 2020; accepted 30 May 2020

Abstract. Self-heating effect for thermomechanical forming processes turns out to be dramatically significant for material with a very low melting point, such as zinc alloys. Zinc low melting point temperature (419.54°C) accentuates metallurgical effects when it is formed in cold or warm manufacturing processes. During deformation, self-heating can therefore induce a relative softening in the behavior law (that could improve formability) which competes with the conventional plastic hardening of the material. Hence, the correct identification of zinc material behavior has to account for both softening and hardening phenomena. This paper studies the effect of plastic work energy in the material identified by means of tensile tests by combining digital image correlation and infrared thermography technique.

Keywords. Self-heating; inverse method; behavior law; plastic work energy.

1. Introduction

Zinc has been applied for building products since 1811. The first ever rolled zinc panel was tested for roofing of the church of St Bartholomew in Liège. Nowadays, zinc is used standardly for claddings, facades, rainwater systems and many other building accessories. The material characteristics of zinc alloys are also interesting for complex structures as well as for ornament applications. To increase the forming of zinc sheet, traditional processes implies the use of pre-heating. The transitional metallurgical temperature of Zinc ($\approx$73.2°C) during cold forming is rapidly reached due to self-heating.

A numerical sensitivity study of the Taylor–Quinney factor [1] was conducted in order to improve the numerical modelling published by [2]. Because of more and more restrictive norms in building, the material performances and product processes must be constantly improved. In a standard production, high velocities and severe stresses are relatively detrimental for anisotropic materials with high sensitivity to strain rates and temperatures [3], which is the case for zinc alloys. The anisotropic viscoplastic behavior of zinc subjected to experimental loading conditions were studied [2, 4]. Strain rate in standard production can reach values over 10 s^{-1}, which involves thermomechanical effects, inducing significant evolutions of the microstructure, as demonstrated by [4]. The microstructure evolution for zinc during forming processes is detailed further by [5] with metallographic observations and mechanical tests. A phenomenon, highlighted but not deeply studied, is the self-heating of zinc. Jansen [4] studied the local measurement of temperature during tensile tests (figure 1). An elevation of 33°C has been measured which brings the deformation into the warm domain of zinc transformation. The 0.5 T_m (melting temperature) of zinc is defined by a very low threshold (T_m = 73.2°C) bringing some microstructural changes very early during transformation stages.

Likewise in any other thermomechanical process, a fraction of the plastic work is dissipated, but the rest of this plastic energy is transformed into heat, increasing the temperature of the material. This phenomenon is called self-heating and is the direct consequence of plastic work energy conversion into heat. To measure the amount of this conversion, [1] proposed a coefficient β, assumed to be relatively constant. This coefficient is defined by the ratio between the thermoplastic heating $\dot{Q}_P$ and the plastic work rate $\dot{W}_P$. From the energy balance equation given by:

$$\rho C_p \frac{dT}{dt} = \beta\sigma : \dot{\varepsilon}_p + k\,\mathrm{div}(\mathrm{grad}T) \qquad (1)$$

where $\boldsymbol{\sigma}$ is the stress tensor, $\dot{\boldsymbol{\varepsilon}}_p$is the plastic strain rate tensor, ρ is the material density (kg m^{-3}), C_p is the specific heat (J kg^{-1} K^{-1}), the Taylor–Quinney factor β is simplified by considering adiabatic conditions, for which no

*For correspondence
Published online: 27 July 2020

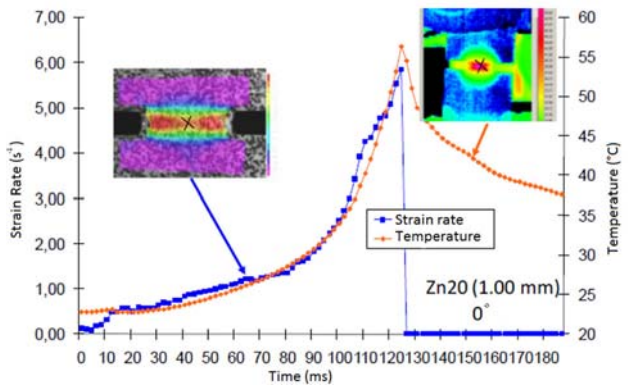

Figure 1. Correlation between local self-heating effect and local strain rate for a plane strain tension test [4].

thermal transfer with the external environment exists. In adiabatic conditions, equation (1) gives:

$$\beta = \frac{\dot{Q}_P}{\dot{W}_P} = \frac{\rho C_p \Delta T}{\int_0^{\bar{\varepsilon}_p} \bar{\sigma} d\bar{\varepsilon}_p} \tag{2}$$

where $\bar{\sigma}$ is the equivalent stress and $\bar{\varepsilon}_p$, the equivalent strain. This equation is used to determine experimentally the Taylor–Quinney factor. It is important to highlight that the adiabatic condition is only valid for thermomechanical process where the plastic strain rate is very high, which does not allow thermal exchanges to take place. To gauge pragmatically the importance of diffusion, the Fourier number F_0 is commonly used. Its expression is given by:

$$F_0 = \frac{\alpha t_C}{L_C^2} \tag{3}$$

where L_C is the characteristic length of the sample defined by the volume of the studied zone over the surface of thermal exchange. t_C is the characteristic time of the phenomenon needed to achieve a critical strain relative to irreversible phenomena. α is the thermal diffusivity equals to 36.3 10^{-5} m^2 s^{-1} for zinc ZnCuTi. Thermomechanical parameters of ZnCuTi, substantially different from pure Zinc, are listed in table 1.

Zehnder *et al* [7] defined a process as adiabatic when the Fourier number F_0 is smaller than 0.01. On the other hand, for $F_0 > 10$ the process is essentially isothermal. For non-adiabatic conditions, [7] proposed a hybrid experimental-numerical procedure to calculate this factor. The results indicate a high dependence of the Taylor–Quinney factor to

Table 1. Thermomechanical parameters of ZnCuTi [6].

Material density ρ (g cm^{-3})	Melting Point T_f (°C)	Specific Heat C_p (J kg^{-1} °C^{-1})	Thermal Conductivity λ (W m^{-1} h^{-1} m^{-2} °C^{-1})
7.17–7.2	420	401.9	104.7

strain. A theoretical model developed by [8] assumed that dislocation multiplications (consequence of strain hardening) are proportional to the rate of increase of the stored energy of cold work. By considering the Hollomon behavior law proposed by [9], the Taylor–Quinney factor becomes:

$$\beta = \frac{\bar{\varepsilon}_p^{1-n} - \bar{h}}{\bar{\varepsilon}_p^{1-n}} \tag{4}$$

with $\bar{h} = \frac{nKh}{E}$, E (MPa) defines the elastic Young modulus, h is a constant which links the stored power and plastic work rate, K is the strength coefficient and n is the hardening coefficient. It seems safe to say that the Taylor–Quinney factor is not constant. It can be linked to the strain rate as discussed in [10]. Ravichandran *et al* [11] proved the dependence of the Taylor–Quinney factor on high strain rates by means of the Kolsky (split-Hopkinson) pressure bars for aluminum and α-titanium. Aluminum seems to be not dependent from strain rate. On the contrary, for α-titanium (a hexagonal crystal lattice material as zinc), the behavior law highly depends on strain rate and demonstrated the high sensitivity of the Taylor–Quinney factor with respect to strain and strain rate (from 1 to 3000 s^{-1}). For magnesium, [12] also proved the dependence of such a Taylor–Quinney factor which β = 0.9–0.95 for high strain rates and β = 0.73–0.75 for intermediate strain rates. For low strain rates, values of β = 0.6–0.7 are used for magnesium as referenced by [3]. To take into account this dependence with the strain rate, [13] proposed the following equation:

$$\beta(\dot{\bar{\varepsilon}}_p) = \beta_0 \left[1 - e^{-\left(p\frac{\dot{\bar{\varepsilon}}_p}{\dot{\varepsilon}_0}\right)^q}\right] \tag{5}$$

with β_0, p, $\dot{\varepsilon}_0$ and q, material parameters.

The identification of a behavior law from the Taylor–Quinney factor requires to adapt the adiabatic stress-strain curves to obtain accurate material parameters. Hor *et al* [14] studied a wide range of strain rates for forging and machining applications and for two grades of steel and aluminum [15]. A softening due to self-heating for steel, as

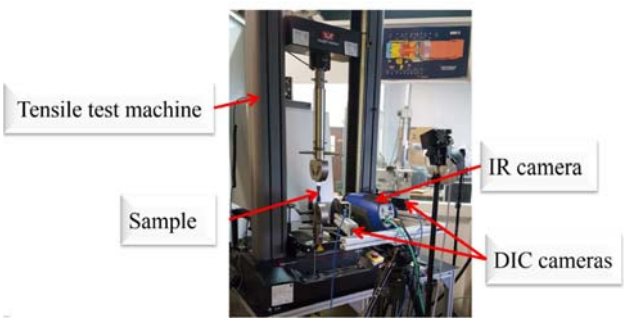

Figure 2. Experimental set-up.

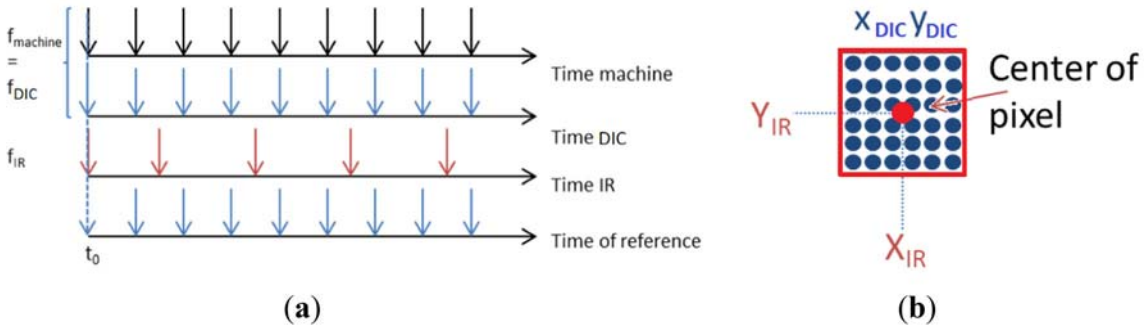

Figure 3. Differences between frequency acquisitions and b) Precision of pixels of both DIC and IRT systems.

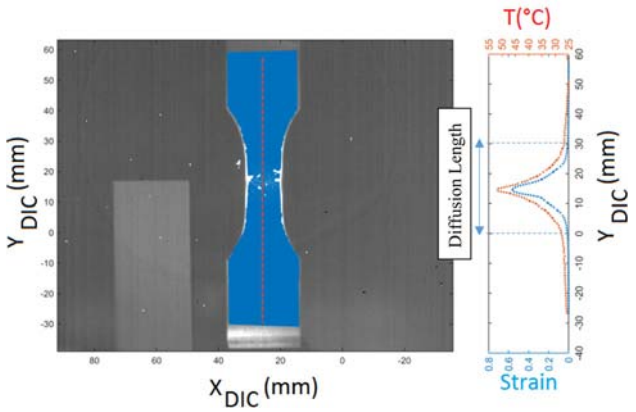

Figure 4. Overlapping of the IR and DIC curves with the temporal and spatial algorithm.

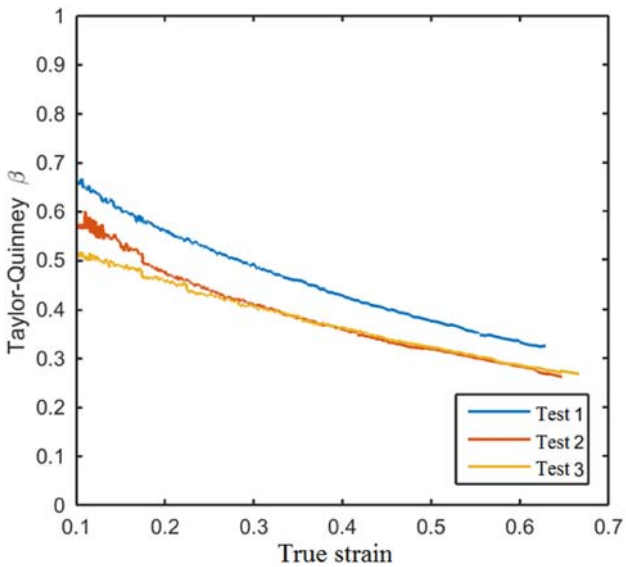

Figure 5. Calculation from 3 tensile tests of the Taylor–Quinney factor following eq. (2) for strain rate equals to 0.1 s^{-1}.

well as aluminum has been identified for temperatures even below 0.3 T_m, which constitutes the cold deformation domain. The author described the identification of the Johnson-Cook behavior law parameters by the need of isothermal stress-strain curves (to obtain the real hardening). From experimental compression tests, numerical simulations were fitted to consider the real adiabatic conditions of the experimental tests (the Taylor–Quinney factor has been fixed to 0.95). Meyer *et al* [13] proposed an experimental methodology to calculate isothermal stress-strain curves from adiabatic experimental conditions to identify the Zerilli-Armstrong behavior law parameters. The authors obtained the experimental isothermal stress-strain curves by unloading every successive step after 8% of deformation until 60% to avoid the self-heating. The authors obtained good agreements with experimental data for strain rate varying between 10^{-3} and 1000 s^{-1}. Another approach was proposed by [16] to fit the behavior at different temperatures. For isothermal conditions, a Cowper–Symonds strain hardening model was proposed. For non-isothermal conditions, a strain rate and temperature dependent hardening response based on a modified Nadai model was used as described by [17].

In this introduction, different approaches were presented to take into account the dependence of thermal effect in the mechanical calculation explicitly or implicitly by the means of the energy balance equation and the determination of the Taylor–Quinney factor. The following part of this article will describe the experimental set-up used to determine the Taylor–Quinney factor and the mechanical conditions for which this factor can be efficiently determined. The second part will present two methods to identify the material parameters from tensile tests data and the influence of the Taylor–Quinney parameter in the numerical calculations.

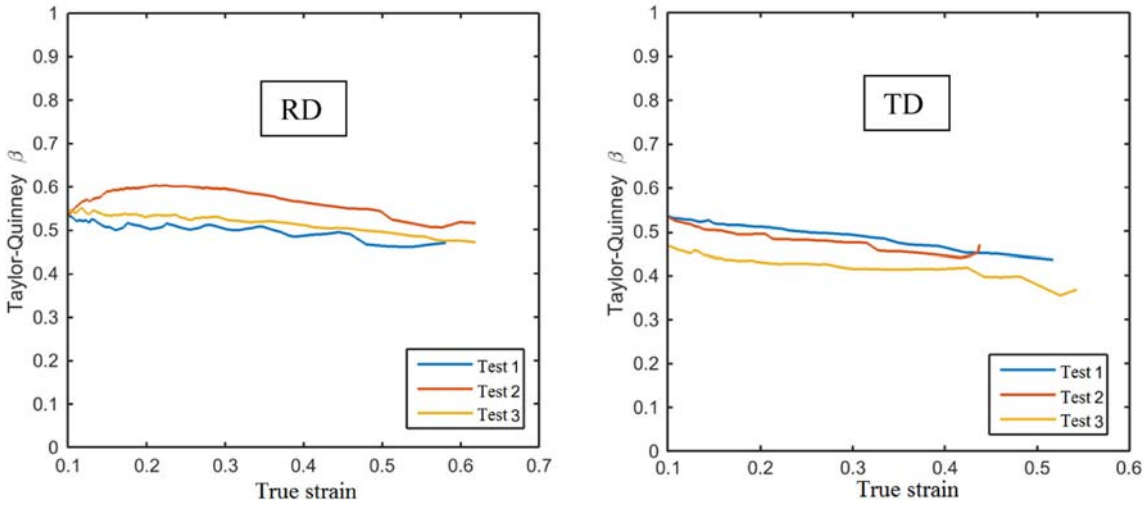

Figure 6. Calculation from 3 tensile tests of the Taylor–Quinney factor for strain rate equals to 0.6 s^{-1} for RD and 1 s^{-1} for TD.

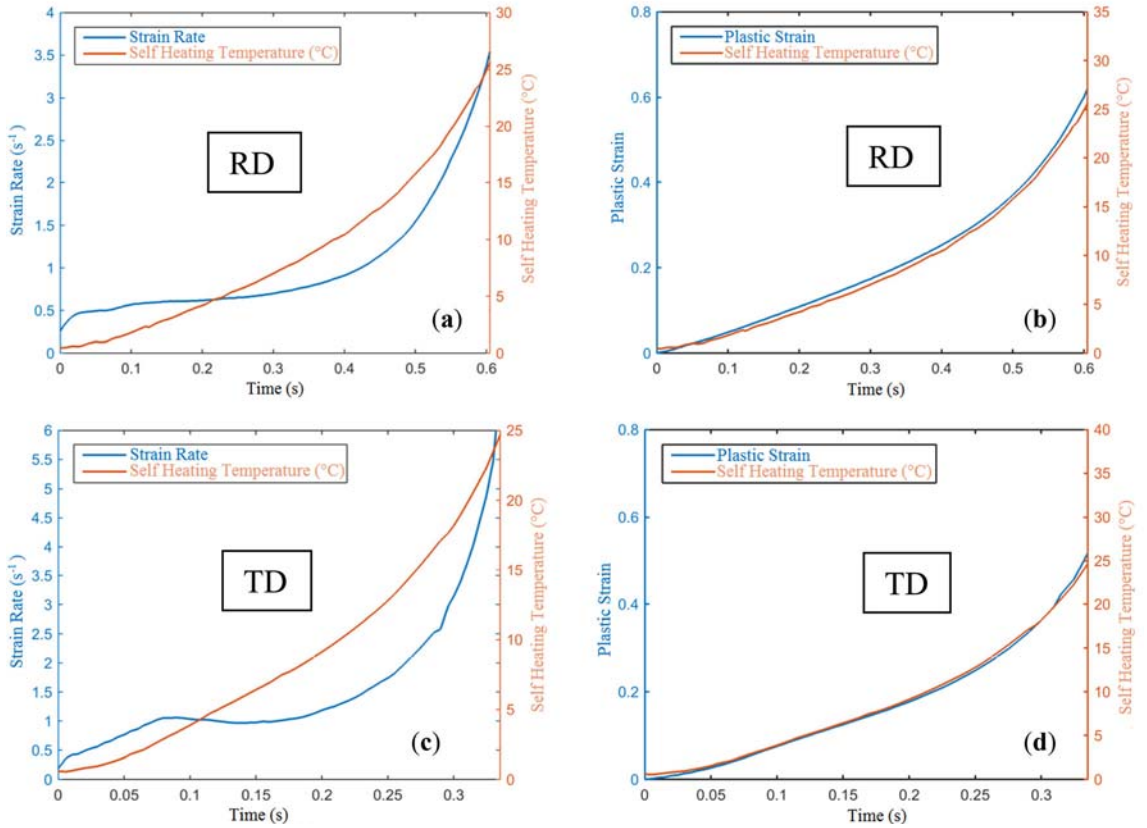

Figure 7. a) and c) Overlapping of strain rate and self-heating temperature versus time; $\dot{\bar{\varepsilon}}_p = 0.6s^{-1}$ b) and d) Overlapping of plastic strain and self-heating temperature versus time; $\dot{\bar{\varepsilon}}_p = 1s^{-1}$.

2. Experimental characterization of self-heating

The studied zinc alloy is a commercial ZnCuTi alloy produced for a standard 0.65 mm thickness. In the present work, the experimental procedure, tackling the correlation between strains and temperatures, is close to the one zpublished by [18]. The experimental set-up is shown in figure 2. The tensile machine is an Instron 5967 (30 kN) coupled with a thermal chamber. The system of Digital Image Correlation (DIC), which is a commercial system of

stereo-correlation, and the Infrared Thermography Technique (IRT) are placed on the same support to be at the same distance from the sample. The DIC cameras (2-point gray grasshopper with 50 mm objectives Schneider Kreuznach) allow the evaluation of displacement fields from which strains are calculated with Hencky assumption. The methodology proposed by [19] was applied in order to analyze the sensitivity of DIC parameters (step, subset, filter size). The optimal set of parameters is given for subset equal to 17, step equal to 5 and filter size equal to 5. The infrared thermography camera (FLIRSC5200) measures the temperature fields by recording the thermal radiation and has been calibrated from a black body with an emissivity close to 1.

A constant velocity of the crosshead is applied, and three velocities were chosen to define the experimental campaign: 0.02 mm/s, 2 mm/s and 12 mm/s corresponding in the RD direction to the following strain rates: 0.001 s^{-1}; 0.1 s^{-1} and 0.6 s^{-1}. For the TD direction, the corresponding strain rates are 0.001 s^{-1}; 0.16 s^{-1} and 1 s^{-1}. Three temperatures were also chosen: 23°C, 80°C and 100°C. 80°C is the temperature used in the industrial forming processes to increase zinc sheets formability.

Standard zinc alloy specimens (in accordance with the ISO 6892-1:2009 standardization) with a prescribed geometry were machined to perform all tests on the same apparatus (10 × 12 mm^2). To obtain efficient measure from IRT, the surface of the sample requires an emissivity close to that of black body and to acquire the strain field from DIC system, random speckle is needed. Therefore, inspired from the [20] work, all specimens were painted in black (for the IRT system) with random white dots (for the DIC system) to correlate, on the same specimen face, strains (obtained by DIC cameras) and temperatures (obtained by the IR camera).

Acquisition frequencies and resolution are different between the DIC and the IRT systems. Spatial and temporal synchronizations were required to compare strain and temperature fields. To schematize the frequencies of sampling, figure 3 a) gives an overview of the frequency discrepancies of each system. The DIC system frequency is higher than the IR frequency. An interpolation is therefore needed to synchronize both systems.

An algorithm was then developed to associate each IRT data to DIC data by interpolating those which are missing. The very first point of the acquisition is measured at the same instant since the three systems (machine, DIC, IRT) were triggered at the same time. For temperature, the interpolation follows this equation:

$$T\left(t^{DIC}\right) = T\left(t^{DIC}\right) + \left(T\left(t_{i+1}^{IRT}\right) - T\left(t_{i}^{IRT}\right)\right)\frac{t^{DIC} - t_{i}^{IRT}}{t_{i+1}^{IRT} - t_{i}^{IRT}} \quad (6)$$

Regarding spatial differences, the resolution of the DIC system (2048 × 1536 pixels) is higher than the resolution of the IR system (320 × 256 pixels). Therefore, one pixel, representing local temperature measured with the IRT system, was associated to 36 DIC pixels (figure 3 b). The methodology has been validated by superimposing the temperature curves related to the infrared response to the strain given by the DIC system on a vertical Y axis passing through the center of sample. This validation is shown in figure 4.

For the calculations of β, the true stress-strain curves in the localization zone were considered. The initial temperature is measured on the specimen near the clamp jaws of the tensile test machine. The isothermal state has been verified for the strain rate equal to 0.001 s^{-1} for which the temperature increase is less than 1°C.

Assuming the different regimes defined by equation (3), the strain rate equals 0.1 s^{-1} indicates a transitional state with F_0 = 0.08. This value was calculated by considering the characteristic length equals to the diffusion length given by the bell curve of temperature as seen in figure 4 (30 mm). The characteristic time was assessed to be the same time related to the time of the utter deformation, which is equal to 4 s in RD and 2 s in TD. Figure 5 indicates the calculation of β for 3 tests. It can be observed that β values

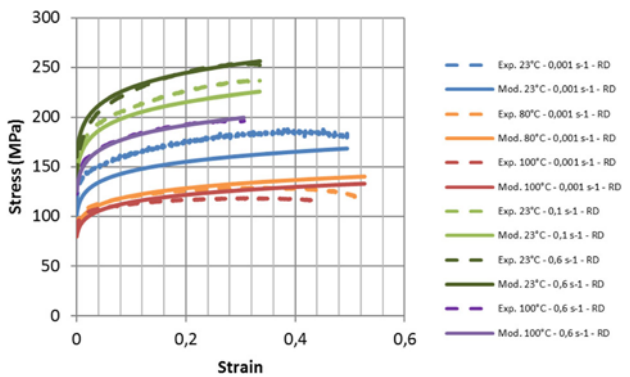

Figure 8. Identification of the material parameters in the RD direction: Exp. for experimental data and Mod. for identified curves obtained by inverse method.

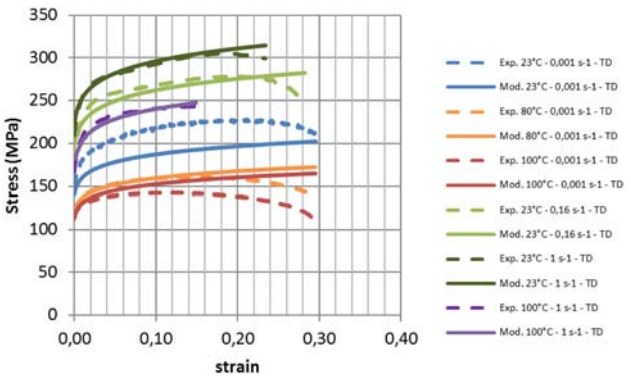

Figure 9. Identification of the material parameters in the TD direction: Exp. for experimental data and Mod. for identified curves obtained by inverse method.

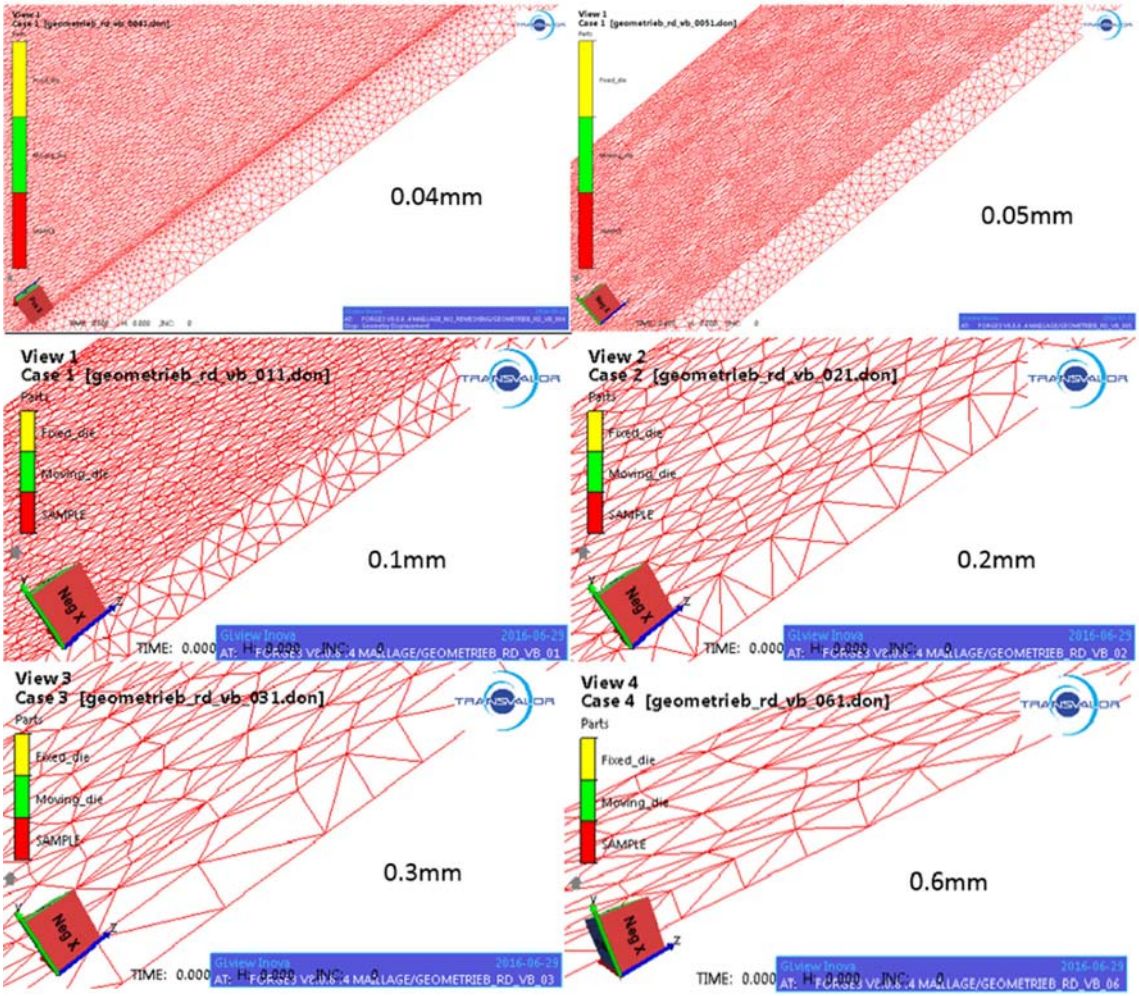

Figure 10. Mesh size sensitivity varying between 0.04 mm (finer) and 0.6 mm (coarser) for the numerical simulations.

Table 2. Numerical results of the mesh sensitivity.

Mesh size	0.04	0.05	0.1	0.2	0.3	0.6
Numerical strain	0.45	0.45	0.45	0.44	0.433	0.415
Strain error (%)	0	0.05	1.12	2.50	3.77	7.88
Time calculation	49 h 56 min 47 s	17 h 45 min 24 s	54 min 30 s	5 min 50 s	1 min 39 s	26 s
Number of mesh elements	2,394,138	1,378,708	205,809	36,842	15,754	4282

are decreasing without reaching a stable state, which is characteristic of the transition state as also described by [7]. The characteristic time is too high to obtain a Fourier coefficient sufficiently low.

Figure 6 shows the results of the calculation of Taylor–Quinney factor for a higher strain rate. The Fourier factor is near 0.02 in RD and 0.03 in TD, which induces a quasi-adiabatic state. The characteristic time is equal to 0.6 in RD and 0.33 in TD. Values of β in the RD and TD directions were identified: $\beta_{RD} = 0.5$ and $\beta_{TD} = 0.44$. A significant anisotropy has been found.

Figure 7 shows the correlation between strain rate and plastic strain versus self-heating temperature in the RD and TD direction. An excellent correlation (for both directions RD and TD) can be noted between plastic strain and self-heating temperature. However, the correlation between strain rate and temperature is not correctly established. The tendency is probably due to the averaged data used to estimate the strain rate from the DIC with a non-optimized time step.

The self-heating temperature can reach 25°C which is very high compared to the 0.5 T_m = 73.2°C.

Table 3. Numerical parameters tested for the identification procedure.

	T (°C)	$\dot{\varepsilon}$ (s^{-1})
Numerical calculation 1	23	0.001
Numerical calculation 2	80	0.001
Numerical calculation 3	100	0.001
Numerical calculation 4	23	0.1
Numerical calculation 5	23	1
Numerical calculation 6	100	1

3. Behavior law identification

Behavior laws parameters were identified from thermo-mechanical tests by the minimization of a cost function. The standard identification procedure is given by minimizing the cost function:

$$\varphi = \frac{1}{N}\sqrt{\sum_{i=1}^{N}\frac{\left(\sigma_i^{\mathrm{mod}} - \sigma_i^{\mathrm{exp}}\right)^2}{\left(\sigma_i^{\mathrm{exp}}\right)^2}} \tag{7}$$

Table 4. Material parameters identified with the global-local MOOPI approach compared to the GRG standard method.

	Anisotropic direction	ε_0	K (MPa)	n	m	β' (K^{-1})	φ_{Moopi}
MOOPI identification	RD	0.002	44.50	0.122	0.0738	404.02	0.607
	TD	0.002	33.12	0.091	0.0533	540.63	1.160
GRG identification	RD	0.002	50.63	0.091	0.0711	346.05	–
	TD	0.002	72.19	0.072	0.0663	293.15	–

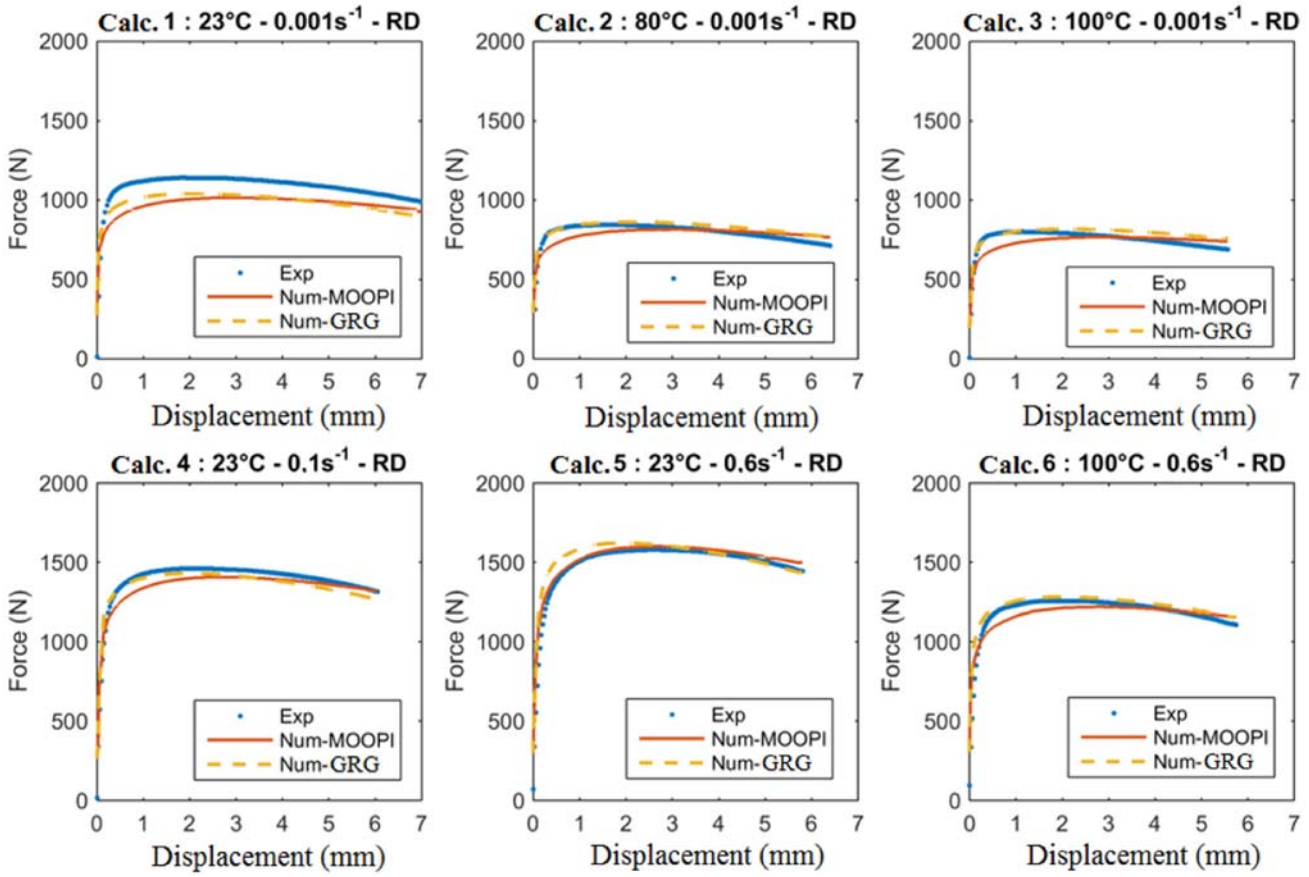

Figure 11. Comparison between force displacement curves obtained by the two identification methods and those obtained experimentally.

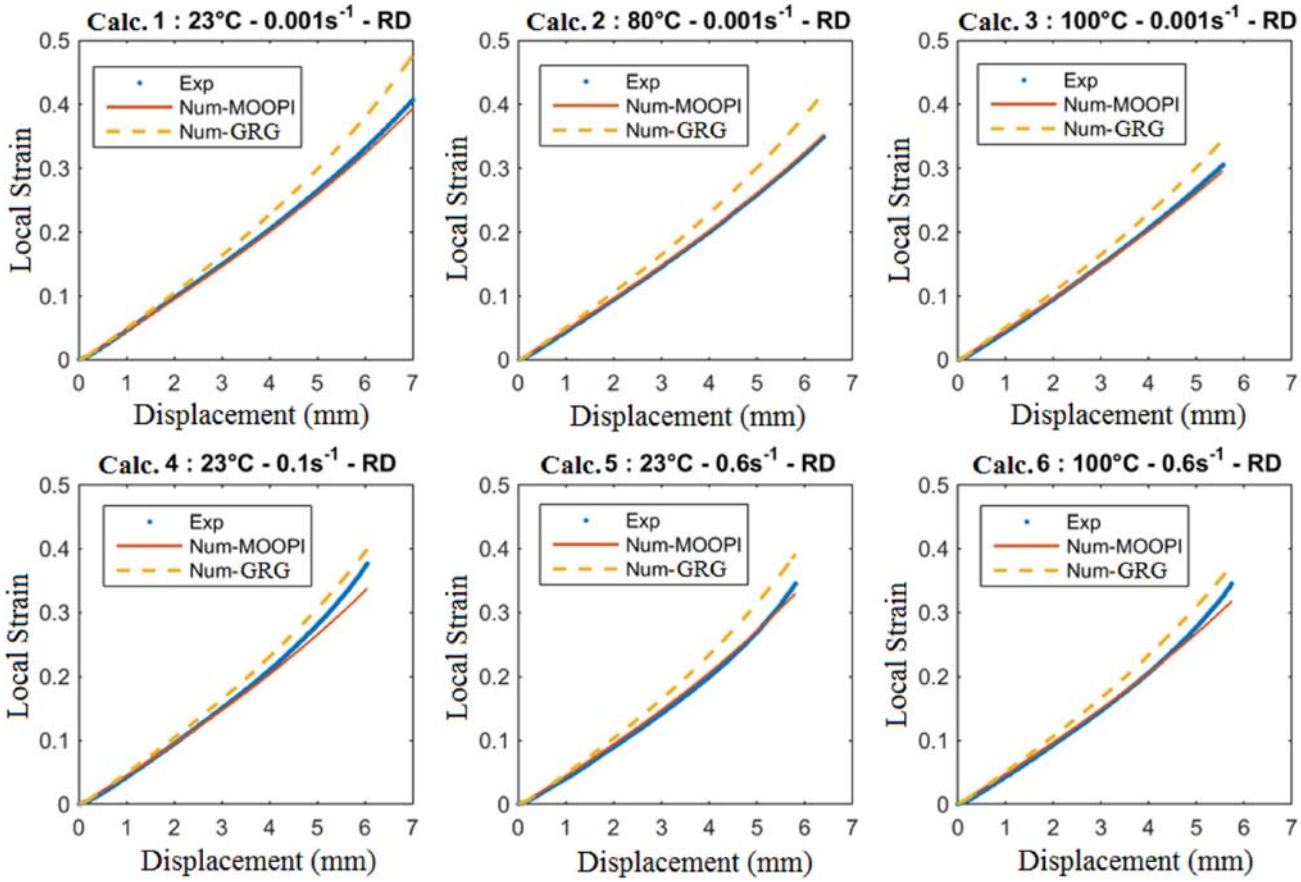

Figure 12. Comparison between local strain - displacement curves obtained by the two identification methods and those obtained experimentally.

where N defines the number of experimental measure points, σ_i^{mod} and σ_i^{exp} are, respectively, the stress calculated with the theoretical behavior law and the experimental stress. Six experimental conditions were tested for both orientations with respect to the rolling direction (RD for rolling direction and TD, the transverse direction). The global cost function is then defined by:

$$\varphi_{Global} = \sum_{i=1}^{k} \varphi_i \tag{8}$$

where k is the number of experimental curves. The global cost function φ_{global} is defined by the sum of all cost functions associated to the different i experimental conditions. In the following equation, the viscoplastic law given by [4] is considered:

$$\bar{\sigma} = \sqrt{3}^{m+1} K(\varepsilon_0 + \bar{\varepsilon})^n \dot{\bar{\varepsilon}}^m \exp(\beta'/T) \tag{9}$$

with $\bar{\sigma}$ and $\bar{\varepsilon}$, the equivalent stress and strain, ε_0, the initial plastic strain, $\dot{\bar{\varepsilon}}$ the strain rate, T the temperature, K the strength coefficient, n the hardening coefficient, m the strain rate sensitivity and β' a parameter depending on temperature effects. This behavior law is similar to the one proposed by [2]. The algorithm applied to converge towards the minimum is a Generalized Reduced Gradient (GRG) method, used by [21], with 100 iterations and a precision of 10^{-6}. The results of the identification are plotted in figures 8 and 9. In the TD direction, the identification is less accurate than in the RD direction.

This method is fast but cannot guarantee the unicity of the solutions. Moreover, the optimization is calculated from only one set of observables given by the stress-strain curves, which limits the accuracy. Another identification method has been confronted to the previous one in order to improve the results, especially for local strain accuracy. The goal is to numerically simulate several experimental conditions of a tensile test and minimizing the cost function. Results depend detrimentally on the mesh size. Different mesh sizes were therefore tested to obtain the best compromise between precision and time calculation (figure 10). The tool velocity is 2 mm/s. The local strain, obtained by DIC, is experimentally equals to 0.45. The results of the time calculation are given in table 2.

To limit the calculation time and get accurate results (table 2), a local refinement of 0.3 mm was chosen for the identification procedure. The finite element software used is coupled with an optimization software called MOOPI for

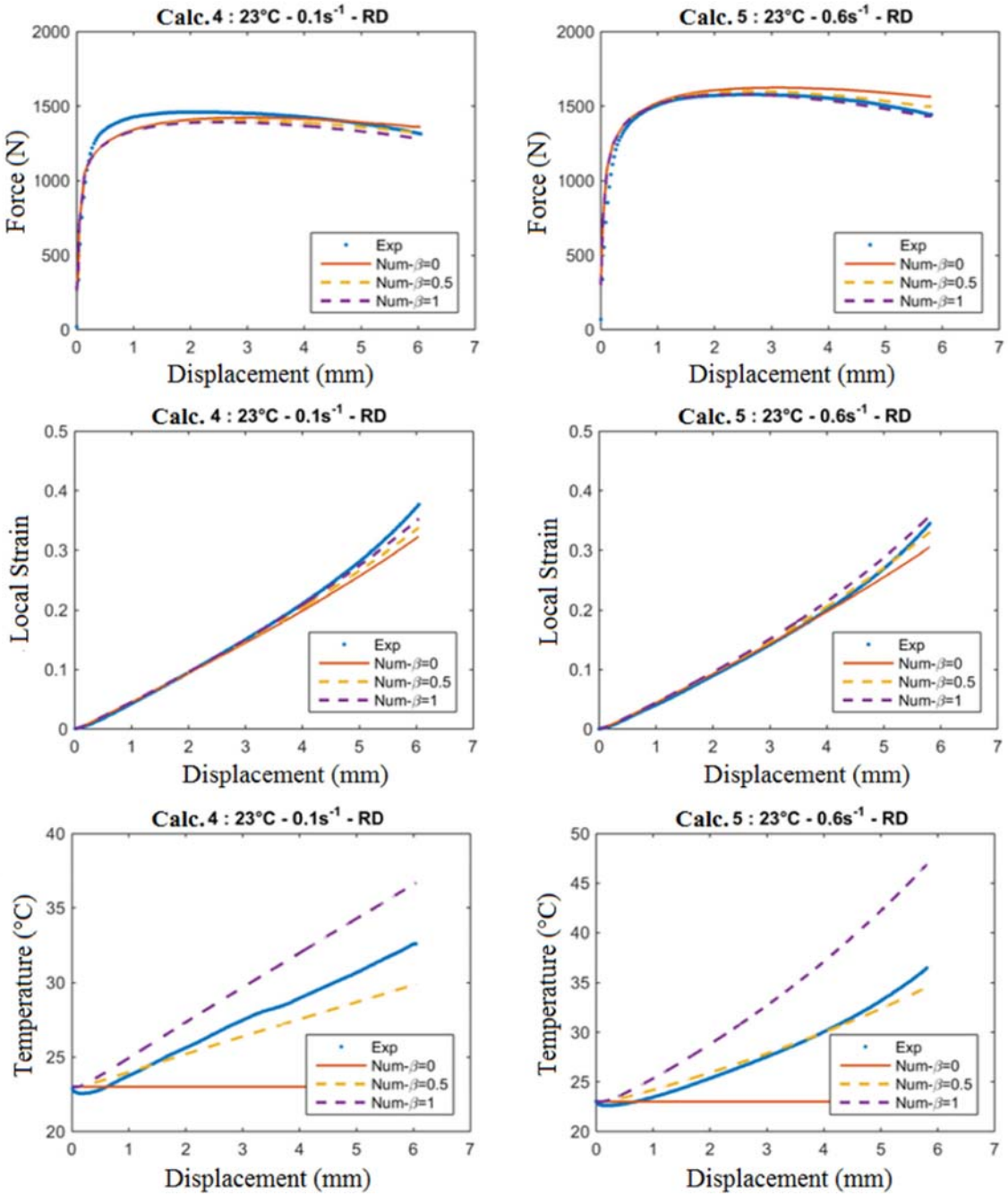

Figure 13. Influence of the Taylor–Quinney factor for numerical calculations.

MOdular Optimization software for Parameters Identification [22]. MOOPI was developed to take into account several numerical tests and different observables. The inverse method used in MOOPI is based on a parallel version of the EGO (Efficient Global Optimization) algorithm and the cost function is defined by:

$$\varphi(P) = \sqrt{\frac{\sum_{i=1}^{N} \left(Obs_i^{num}(P) - Obs_i^{exp}\right)^2}{\sum_{i=1}^{N} \left(Obs_i^{exp}\right)^2}} \tag{10}$$

Table 5. Influence of the Taylor–Quinney factor on the numerical simulations and relative error obtained for the force, local strain and temperature.

		F (N)	Relative error	ε	Relative error	T (°C)	Relative error
T = 23°C	Exp.	1314.42	–	0.376	–	32.61	–
$\dot{\varepsilon}$ = 0.1 S^{-1}	β = 0	1360.22	3.5	0.323	−14.2	23	
RD	β = 0.5	1321.25	0.5	0.338	−10.3	29.91	−8.3
	β = 1	1285.31	−2.2	0.353	−6.3	36.68	12.5
T = 23°C	Exp.	1442.59	–	0.345	–	36.50	–
$\dot{\varepsilon}$ = 0.6 S^{-1}	β = 0	1565.32	8.5	0.305	−11.5	23	−37
RD	β = 0.5	1497.36	3.8	0.330	−4.2	34.54	−5.4
	β = 1	1432.22	−0.7	0.358	3.7	46.9	28.5

where N is the number of measure points, $Obs_i^{num}(P)$ and $Obs_i^{\exp}$ are respectively the values of the numerical and experimental observables and P is the set of tested parameters. Six numerical conditions with different temperatures and strain rates were tested and are summarized in table 3.

The observables used in the minimization of the cost function are both global and local observables. For the global observables, the data used are the force-displacement values. The local observables are identified by local strain and local temperature obtained by collecting numerical data in the necking zone. The global cost function is then given by:

$$\varphi_{Moopi} = \sum_{i=1}^{k} \left(\varphi_i^F + \varphi_i^{\varepsilon}\right) + \varphi_5^T \qquad (11)$$

where k = 1 to 6, the number of numerical calculations. φ_i^F, φ_i^{ε}, ϕ_5^T are respectively the cost function considering the observable related to the force, the strain and the temperature (only for the fifth simulation for which self-heating is relevant). The results stemming from this identification are summarized in table 4.

The numerical force-displacement curves obtained by the two methods are compared to the experimental curves in figure 11 and local strain values are plotted in figure 12. Both numerical methods were identified until the localized necking. The results obtained by the standard method give a better result for the force-displacement curves especially in the vicinity of the yield stress. However, as seen in figure 13, the MOOPI method gives a much better fitting than the standard method for local strain values. It is worth mentioning that the calculation time is much longer for the MOOPI identification (more than 1 day) compared to the GRG method which requires only 5 minutes.

The GRG approach is therefore an efficient method for a fast identification of the material behavior parameters before localized necking. The MOOPI identification gives a more accurate local deformation. This is particularly important for predicting localized necking as well as for the study of final failure.

To verify the experimental values, the influence of the Taylor–Quinney factor has been studied. The goal is also to assess the precision of the numerical calculations, which have been performed only for conditions for which self-heating has been revealed.

There is a little impact on the force-displacement curves and for the determination of the local strain as shown in figure 13. However, the influence on the temperature is tremendous. For a Taylor–Quinney factor equals to 0.5, the temperature has a good fitting compared to the experimental one, while if the Taylor–Quinney factor was fixed to 1 (which is the default choice made standardly in numerical calculations) the result would have been totally false.

Table 5 references all data obtained numerically, and the relative error compared to the experimental values. The best relative errors are obtained for $\beta = 0.5$.

For strain rate values in the range [0.001 s^{-1}; 0.1 s^{-1}] and for temperatures in the range [23°C; 100°C], the experimental value of the Taylor Quiney factor used in numerical simulations fits precisely the experimental curves. However, more numerical simulations are needed to calculate the optimized value of this factor in all configurations.

4. Conclusion

This paper presents an experimental methodology to identify the Taylor–Quinney factor of a standard zinc alloy by means of DIC systems and infrared camera measurements. Specific algorithms were developed to synchronize – in space and time - the acquired data to overlap the strain field and the temperature. The Taylor–Quinney factor has been identified equals to 0.5 in the rolling direction and 0.44 in the transverse direction for a strain rate close to 1 s^{-1}. This anisotropy is not common in the literature. The identification of the material behavior parameters together with a numerical sensitivity analysis have shown a high effect of the Taylor–Quinney factor in the determination of the effective temperature. To assess the influence of this factor on numerical calculations, a behavior law was identified by

means of two different methods: the GRG method, which is the common one, and an inverse analysis methodology carried out with the MOOPI software based on an EGO strategy. Although the GRG method is the fastest, the uniqueness of the solution cannot be proved and global minima cannot be verified. The MOOPI approach, based on evolution strategy algorithms, avoids local minima and gives the best global solution of the minimization problem. This approach is also more accurate thanks to the use of both local and global observables. The fact that MOOPI cannot satisfy both the global and local observables may come from the fact that the material behavior law should be improved in order to model zinc complex behavior and in particular this competition between plastic hardening on one side and self-heating softening on the other side.

The perspective of this work is therefore to apply this identification methodology with an enriched material law, as the one proposed by [17]. This would enable to account for the effect of self-heating directly and explicitly in the mechanical calculation. It will also be interesting to study the evolution of the microstructure linked to the strain rate and the temperature.

References

[1] Taylor G I and Quinney H 1934 The latent energy remaining in a metal after cold working. In: *Proceedings of the Royal Society of London. Series A 143*, pp. 307–326

[2] Milesi M, Logé R E and Jansen Y 2014 Anisotropic behavior and formability criterion for zinc sheets. *J. Mat. Process. Tech.* 214: 2869–2876

[3] Feng F, Huang S, Meng Z, Hu J, Lei Y, Zhou M, Wu D and Yang Z 2014 Experimental study on tensile property of AZ31B magnesium alloy at different high strain rates and temperatures. *Mater. and Design* 57: 10–20

[4] Jansen Y 2013 *Modélisation et optimisation du processus de formage de pièces en zinc*. PhD, MinesParistech, Sophia-Antipolis, France

[5] Pantazopoulos G, Toulfatzis A, Vazdirvanidis A and Rikos A 2017 Fundamental aspects of rolled Zn alloy sheet formability: structure-property and failure mode relationships. *Mat. Sci. Forum, Trans. Tech. Publications* 879: 1443–1448

[6] Porter FC 1991 *Zinc Handbook: Properties, Processing, and Use in Design*, Marcel Dekker, New York

[7] Zehnder A T, Babinsky E, Palmer T 1998 Hybrid method for determining the fraction of plastic work converted to heat. *Exp. Mech.* 8 (4): 295–302

[8] Zehnder A T 1991 A model for the heating due to plastic work. *Mech. Res. Commun*. 18(1): 23–28

[9] Pottier T, Toussaint F, Louche H and Vacher P 2013 Inelastic heat fraction estimation from two successive mechanical and thermal analyses and full-field measurements. *European J. Mech. A/Solids* 38: 1–11

[10] Macdougall D 2000 Determination of the plastic work converted to heat using radiometry. *Exp. Mech.* 40(3): 298–306

[11] Ravichandran G, Rosakis A J, Hodowany J and Rosakis P 2002 On the conversion of plastic work into heat during high-strain rate deformation. In: *Proceedings of AIP Conference 620*, pp. 557–562

[12] Ulacia I, Salisbury C P, Hurtado I and Worswick M J 2011 Tensile characterization and constitutive modeling of AZ31B magnesium alloy sheet over wide range of strain rates and temperatures. *J. Mater. Process. Tech.* 211(5): 830–839

[13] Meyer L W, Herzig N, Halle T, Hahn F and Krueger L 2007 Staudhammer KP. A basic approach for strain rate dependent energy conversion including heat transfer effects: An experimental and numerical study. *J. Mater. Process. Tech.* 182: 319–326

[14] Hor A, Morel F, Lebrun J L and Germain G 2013 Modelling identification and application of phenomenological constitutive laws over a large strain rate and temperature range. *Mech. of Mat.* 64: 91–110

[15] Hor A 2011 *Simulation physique des conditions thermomécaniques de forgeage et d'usinage : caractérisation et modélisation de la rhéologie et de l'endommagement*. PhD, Arts et Métiers Paristech, Angers, France

[16] Ghaffari Tari D and Worswick M J 2015 Elevated temperature constitutive behavior and simulation of warm forming of AZ31B. *J. Mater. Process. Tech.* 221: 40–55

[17] Van Den Boogaard A H 2002 *Thermally Enhanced Forming of Aluminium Sheet: Modelling and Experiments*. PhD, Twente, The Netherlands

[18] Chrysochoos A, Wattrisse B, Muracciole J M and El Kaïm Y 2009 Fields of stored energy associated with localized necking of steel. *J. Mech. Mat. and Struct.* 4(2): 245–262

[19] Candau N, Pradille C, Bouvard J L and Billon N 2016 On the use of a four-cameras stereovision system to characterize large 3D deformation in elastomers. *Polymer Testing* 56: 314–320

[20] Reibez P S 2008 *Influence of thermal and mechanical aspects on deformation behavior of NiTi alloys., Grenoble*: PhD, University of Joseph-Fourier, France

[21] Lasdon L S, Fox R L and Ratner M W 1973 Nonlinear Optimization Using the Generalized Reduced Gradient Method. *Technical Memorandum n° 325, NTIS*

[22] Roux E 2011 *Assemblage mécanique: stratégies d'optimisation des procédés et d'identification des comportements mécaniques des matériaux*. PhD, MinesParistech, Sophia-Antipolis, France